Accepted Manuscript

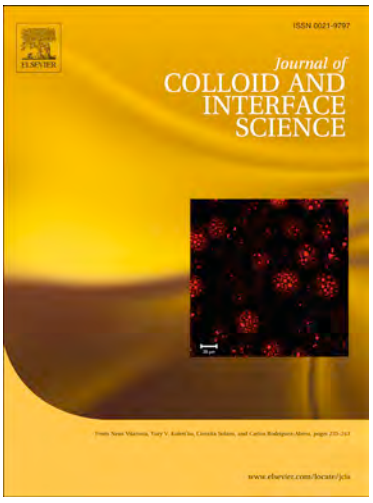

The fabrication of ultrathin films and their gas separation performance from polymers of intrinsic microporosity with two-dimensional (2D) and three-dimensional (3D) chain conformations

Javier Benito, Julio Vidal, Javier Sánchez-Laínez, Beatriz Zornoza, Carlos Téllez, Santiago Martín, Kadhum J. Msayib, Bibiana Comesaña-Gándara, Neil B. McKeown, Joaquín Coronas, Ignacio Gascón

PII: S0021-9797(18)31275-X
DOI: https://doi.org/10.1016/j.jcis.2018.10.075
Reference: YJCIS 24230

To appear in: *Journal of Colloid and Interface Science*

Received Date: 29 August 2018
Revised Date: 19 October 2018
Accepted Date: 24 October 2018

Please cite this article as: J. Benito, J. Vidal, J. Sánchez-Laínez, B. Zornoza, C. Téllez, S. Martín, K.J. Msayib, B. Comesaña-Gándara, N.B. McKeown, J. Coronas, I. Gascón, The fabrication of ultrathin films and their gas separation performance from polymers of intrinsic microporosity with two-dimensional (2D) and three-dimensional (3D) chain conformations, *Journal of Colloid and Interface Science* (2018), doi: https://doi.org/10.1016/j.jcis.2018.10.075

The fabrication of ultrathin films and their gas separation performance from polymers of intrinsic microporosity with two-dimensional (2D) and three-dimensional (3D) chain conformations

Javier Benito[⊥], Julio Vidal[⊥], Javier Sánchez-Laínez[±], Beatriz Zornoza[±], Carlos Téllez[±], Santiago Martín[§], Kadhum J. Msayib[£], Bibiana Comesaña-Gándara[£], Neil B. McKeown[£], Joaquín Coronas[±] and Ignacio Gascón[⊥*]

[⊥]Instituto de Nanociencia de Aragón (INA) and Departamento de Química Física, Universidad de Zaragoza, C/ Pedro Cerbuna 12, 50009 Zaragoza (Spain).

[±]Chemical and Environmental Engineering Department and Instituto de Nanociencia de Aragón (INA), Universidad de Zaragoza, 50018 Zaragoza (Spain).

[§]Instituto de Ciencia de Materiales de Aragón (ICMA) and Departamento de Química Física, CSIC-Universidad de Zaragoza, C/ Pedro Cerbuna 12, 50009 Zaragoza (Spain).

[£]EastChem, School of Chemistry, University of Edinburgh, David Brewster Road, Edinburgh, EH9 3FJ (UK).

Corresponding Author

* Ignacio Gascón, E-mail: igascon@unizar.es, Phone: +34 976761204

Abstract

The expansion of the use of polymeric membranes in gas separation requires the development of membranes based on new polymers with improved properties and their assessment under real operating conditions. In particular, the fabrication of ultrathin films of high performance polymers that can be used as the selective layer in composite membranes will allow large reductions in the amount of the expensive polymer used and, hence, the cost of membrane fabrication.

In this contribution, two polymers of intrinsic microporosity (PIMs) with very different chain configurations (two-dimensional, 2D, chains or conventional contorted three-dimensional, 3D, conformation) have been compared in their ability to form ultrathin films, showing the relevance of polymer design to obtain compact and defect-free films. Monolayers of the 2D polymer PIM-TMN-Trip can be efficiently deposited onto poly[1-(trimethylsilyl)-1-propyne] (PTMSP) to obtain composite membranes with a CO_2/N_2 selectivity similar to that of the corresponding thick membranes of the same PIM using only a small fraction of the selective polymer (less than 0.1%).

Keywords: ultrathin films; polymers of intrinsic microporosity; polymer design; composite membranes; gas separation.

1. Introduction

The industrial use of polymeric membranes in gas separation processes started in the late 1970s and the main applications in this field were developed during the following decade. These applications represent 80-90% of the contemporary gas separation membrane industry [1]. To expand the use of polymeric membranes to other gas separation processes, such as CO_2 capture [2], new materials with improved properties are required [3]. For example, polymers of intrinsic microporosity (PIMs) [4, 5], with exceptionally high free volume, high permeability and moderate selectivity, are very promising candidates for the development of gas separation membranes, especially for CO_2/CH_4 and CO_2/N_2 separations. Membranes fabricated with these new generation polymers should be tested under real gas separation conditions, since generally pure gas measurements involving CO_2 are poor predictors of the ultimate performance during real-world use [3].

Recently [6], we demonstrated that the Langmuir-Blodgett (LB) technique [7] can be used to obtain compact monolayer films of a polymer of intrinsic microporosity, PIM-EA-TB(H_2), at the air-water interface. These monolayers can be then deposited successively onto different solid substrates using the Langmuir-Schaefer (LS) horizontal deposition method [8] to obtain a dense multilayer PIM film of the desired thickness. The deposition of 30 PIM-EA-TB(H_2) monolayers onto poly[1-(trimethylsilyl)-1-propyne] (PTMSP) flat membranes gave an ultrathin PIM layer of only 30 nm in thickness. The PTMSP/PIM-EA-TB(H_2) composite membranes were tested for CO_2/N_2 separation at 35ºC and feed pressures between 1 and 3 bar, and demonstrated a selectivity of 13.5, similar to that obtained with thick membranes of PIM-EA-TB(H_2), with high CO_2 permeance (114 GPU). Therefore, this methodology can be used to

reduce significantly the thickness of the selective layer (and consequently the cost of the membrane) whilst retaining performance.

Here we report the fabrication and characterization of Langmuir, Langmuir-Blodgett and Langmuir-Schaefer films of two more PIMs (the archetypal PIM-1 and the recently reported ultrapermeable PIM-TMN-Trip) in order to analyze the influence of the polymer structure on the ability of these materials to form films using the LB technique and their performance as selective layers for CO_2/N_2 separation. Of particular interest is the very different chain configuration between PIM-1 and PIM-TMN-Trip with the latter designed to possess a 2D chain whereas the former has a conventional contorted 3D conformation (Figure 1).

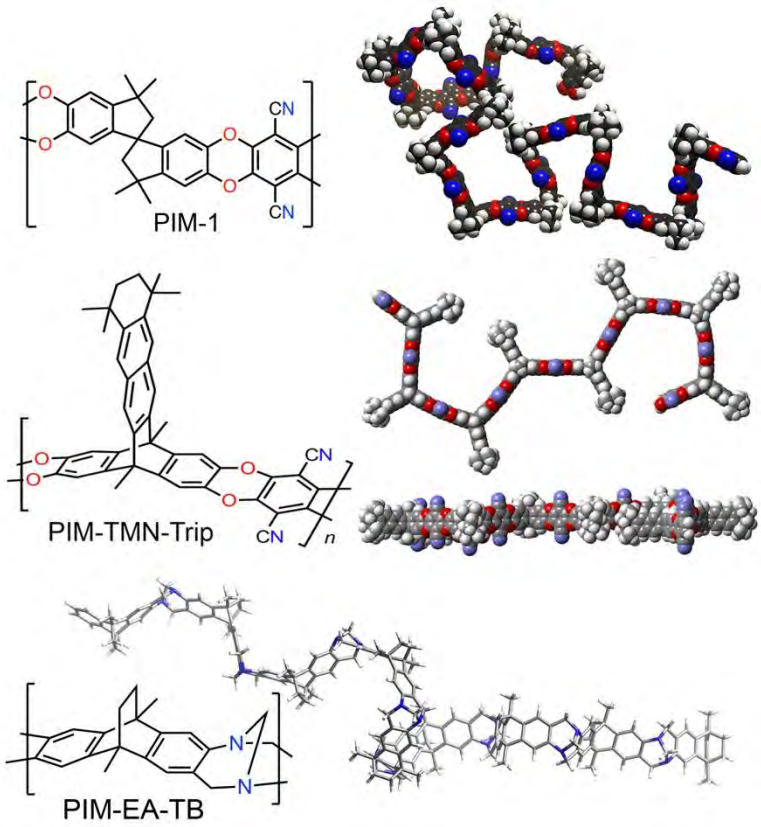

Figure 1. Chemical structures and energy minimized 3D chain conformation of PIM-1 and the 2D chain configuration of the ultrapermeable PIM-TMN-Trip. For comparison, the structure and 3D chain conformation of PIM-EA-TB, structurally similar to PIM-EA-TB(H_2), is also shown.

2. Materials and methods

2.1. PIM synthesis

PIM-1 [9, 10], PIM-EA-TB(H_2) [11, 12], and PIM-TMN-Trip [13] were prepared and characterized using methods reported previously. Molecular masses as measured using gel permeation chromatography relative to polystyrene standards are as follows: PIM-EA-TB(H_2) M_n = 9,300 g·mol^{-1}, M_w = 49,500 g·mol^{-1}; PIM-1 M_n = 110,000 g·mol^{-1}, M_w = 300,000 g·mol^{-1}; PIM-TMN-Trip M_n = 52,000 g mol^{-1}, M_w = 197,000 g·mol^{-1}. Gel permeation chromatography was carried out using a Viscotek GPC Max1000 system which includes a refractive index detector and two columns (Malvern, LT5000L). The analysis used dilute solution of polymer in chloroform (1 mL·min^{-1}).

2.2. PIM film fabrication and characterization

PIM-1 and PIM-EA-TB(H_2) solutions were prepared by dissolving the appropriate amount of the powdered sample in chloroform (HPLC grade purchased from LabScan, 99.8%) and stirring until homogeneous solutions were obtained. In order to obtain solutions of PIM-TMN-Trip, sonication using an ultrasound probe was required before stirring to dissolve completely the polymer. The concentration of the solutions (4×10^{-5} M for PIM-1, 1.5×10^{-4} M for PIM-EA-TB(H_2) and 1×10^{-5} M for PIM-TNM-Trip) was calculated using the molar masses of the repeat unit of the polymers. The ultrasound probe-type device used for PIM-TMN-Trip was a Hielscher UP400S ultrasonic processor (Power Output 400 W) equipped with an H3 type tip (3 mm diameter).

Polymer film formation at the air-water interface and its characterization by surface pressure (π) and surface potential (ΔV) vs. area (A) isotherms and Brewster Angle microscopy (BAM) were carried out in a commercial Langmuir Teflon trough, NIMA

model 702, with dimensions of 720 mm × 100 mm, equipped with two symmetric barriers. Langmuir-Blodgett (LB) and Langmuir-Schaeffer (LS) films were fabricated using a KSV-NIMA trough, model 2000-System 3, with dimensions 775 × 120 mm and a symmetrical double-barrier system. Both troughs were kept inside a closed cabinet in a clean room at constant temperature (20 ± 1°C). Ultra-pure Milli-Q water (ρ = 18.2 MΩ·cm) was used in all the experiments as subphase. Surface pressure (π) was continuously monitored using a Wilhelmy balance with a filter paper plate. Surface potential measurements were performed with a KSV Nima Spot Surface Potential Sensor. BAM images were obtained with a KSV NIMA Micro BAM using a red laser (50 mW, 659 nm) as light source with a fixed incidence angle of 53.1º and with a spatial resolution of the optical system in the water surface plane of 6 mm per pixel.

In each experiment, the appropriate volume of the PIM solution was spread drop by drop using a gas-tight Hamilton microsyringe held very close to the water surface and allowing the surface pressure to return to a value close to zero between each addition. After spreading, the solvent was left to evaporate for 15 min before starting the compression, which was performed at a constant compression speed of 6 $cm^2 \cdot min^{-1}$. Both π-A and ΔV-A isotherms were registered at least three times to check the reproducibility of the results.

LB films were transferred on solid substrates (quartz and mica) initially immersed into the aqueous subphase at the desired surface pressure using the vertical dipping method at a vertical speed of 1 $mm \cdot min^{-1}$. To fabricate Langmuir-Schaefer films, the substrates were held horizontally and parallel to the water surface using a vacuum pump-based horizontal dipping clamp (KSV KN-0006). When the desired surface pressure was reached, the substrate was approached to the surface at a vertical speed of 1 $mm \cdot min^{-1}$. Once the substrate contacted the water surface, it was withdrawn at 10 $mm \cdot min^{-1}$; after

each deposition, the samples were dried with N_2 at ambient temperature before characterization or successive depositions.

Atomic force microscopy (AFM) images were obtained in tapping mode using a Multimode 8 microscope equipped with a Nanoscope V control unit from Bruker operating under ambient air conditions at a scan rate of 1 Hz. To this end, RTESPA-150 (90-210 kHz, and 5 $N \cdot m^{-1}$, nominal tip radius of 8 nm), purchased from Bruker, was used.

UV-vis spectra of the PIM solutions and LB and LS films deposited on quartz substrates were recorded at a normal incident angle with respect to the film plane in a Varian Cary 40 Bio spectrophotometer.

2.3. PTMSP/PIM composite membrane fabrication

PTMSP/PIM-TMN-Trip and PTMSP/PIM-1 composite membranes were prepared by depositing the desired number of PIM monolayers onto PTMSP supports at constant surface pressure using the LS method, dried with N_2 at ambient temperature and used without any further modification for gas separation studies.

For the preparation of PTMSP supports of ca. 80 μm thickness, the polymer (purchased from Cymit Quimica, >95%) was first dissolved at 1.87 wt.% concentration in toluene (analytical reagent purchased from VWR Chemicals, >99.5%) at room temperature. Then, the solution was poured into a glass Petri dish and allowed to dry during 72 h at room temperature. The obtained sheets were immersed in methanol (purchased from Sigma-Aldrich, 99.8%) for 24 h to remove traces of toluene. Before use, the PTMSP supports were gently dried with paper sheets.

2.4. Gas separation measurements

Dense and composite membranes were cut in circular areas of 2.12 cm^2 for gas separation studies. These studies were performed at 35 °C and two different feed pressures (1 and 3 bar). The membranes were assembled into a module consisting of two stainless steel pieces and a 316LSS macroporous disk support (from Mott Co.) with a 20 μm nominal pore size, gripped inside with Viton O-rings. The permeation module was placed in a UNE 200 Memmert oven to control the temperature of the module. Gas separation measurements were carried out by feeding a 10/90 in volume CO_2/N_2 mixture (100 $cm^3(STP)\cdot min^{-1}$) to the feed side by means of two mass flow controllers (Alicat Scientific, MC-100CCM-D), while the permeate side of the membrane was swept with a 4.5 $cm^3(STP)\cdot min^{-1}$ mass flow controlled stream of He at 1 bar (Alicat Scientific, MC-5CCM-D). The maximum total permeate flux obtained during these measurements was near 0.60 $cm^3(STP)\cdot min^{-1}$, which would imply a CO_2 stage cut of 0.06 $cm^3(STP)\cdot min^{-1}$. This value is small enough to assume that permeate fluxes are negligible as compared to feed and retentate fluxes. Permeate concentrations of CO_2 and N_2 were analyzed online by an Agilent 3000A micro-gas chromatograph equipped with a thermal conductivity detector (TCD). Permeance was calculated in GPU (10^{-6} $cm^3(STP)/(cm^2\cdot s\cdot cmHg)$) once the steady-state was reached (after about 3 h). The separation selectivity was obtained as the ratio of CO_2 and N_2 permeances. At least 2 membrane samples of each type were fabricated and measured to provide the corresponding error estimations.

Images of polymeric membranes fabricated in this work and the module used for gas separation studies can be found in the Supplementary Material (Figure S1).

3. Results and discussion

3.1. PIM films at the air-water interface

Figure 1 shows the chemical structures of the PIMs (PIM-TMN-Trip and PIM-1) used to fabricate ultrathin films. As can be observed, the ultrapermeable PIM-TMN-Trip is based on the triptycene unit (Trip) with a tetramethyltetrahydronaphthalene (TMN) as the extended substituent. The role of TMN is to enhance the 2D aspect ratio of the polymer chain and to improve the solubility of the polymer [13]. The well-known PIM-1 is based on the relatively flexible spirobisindane (SBI) moiety and presents a 3D contorted structure [10]. Finally, the previously studied PIM-EA-TB(H_2) [6], structurally similar to PIM-EA-TB [11, 12], also has a 3D contorted chain structure consisting of ethanoanthracene (EA) units fused together by Tröger's base (TB).

Figure 2 shows the surface pressure-area isotherms of PIM-1 and PIM-TMN-Trip studied in this contribution as well as that of the previously reported PIM-EA-TB(H_2) [6], for comparison. The surface pressure-area isotherms for the three polymers present some similarities although the areas per monomer are clearly very different. After the lift-off in the π–A isotherm, that takes place at 1.34 (PIM-TMN-Trip), 0.74 (PIM-EA-TB(H_2)) and 0.20 nm^2 per monomer (PIM-1), the surface pressure rises gradually during compression until an increase in the slope and a monotonous increase of the surface pressure upon further compression is observed. This change in the slope is generally associated with a phase transition to a more condensed phase of the film and takes place at the following areas per monomer: 0.83 nm^2 (PIM-TMN-Trip), 0.37 nm^2 (PIM-EA-TB(H_2)) and 0.17 nm^2 (PIM-1). Finally, at higher surface pressures, a decrease in the slope, that could indicate a partial collapse of the film, is observed at 0.53 nm^2 (PIM-TMN-Trip), 0.25 nm^2 (PIM-EA-TB(H_2) and 0.14 nm^2 (PIM-1). This behavior reflects the different chemical structure of the polymers: the 2D macromolecular chains of PIM-TMN-Trip [13] take up a larger area at the air-water interface than the PIM-EA-TB(H_2) chains which form a series of rigid rods (the bridged

bicyclic rings) connected to each other, as was detailed for the structurally similar polymer PIM-EA-TB [12]. Finally, the PIM-1 contorted 3D chains present the lower area per monomer of the three polymers analyzed.

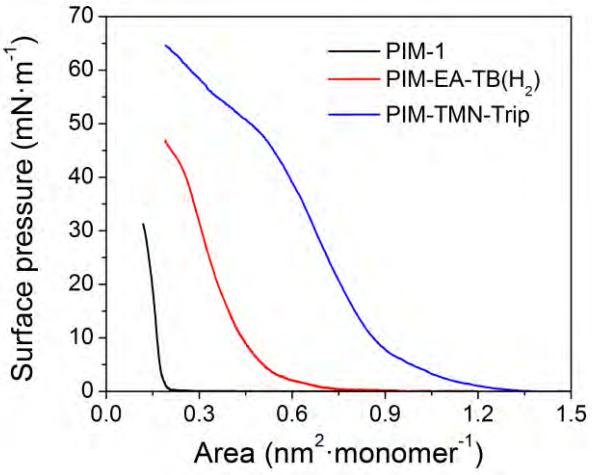

Figure 2. Surface pressure-area (π-A) isotherms for the different PIMs studied.

The surface potential vs. area per monomer isotherms were also registered for the three PIMs in order to obtain further information about the organization of the films at the air-water interface (Figure 3). Positive surface potential values were obtained for PIM-1 and PIM-EA-TB(H_2), whilst these are slightly negative for PIM-TMN-Trip. Additionally, for PIM-EA-TB(H_2) significantly higher surface potential values than for PIM-1 were observed.

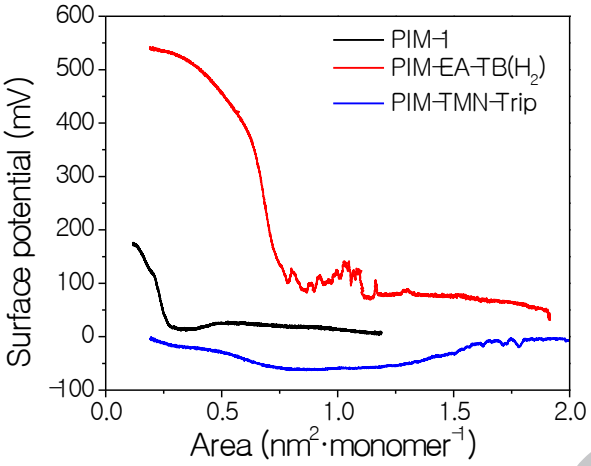

Figure 3. Surface potential-area (ΔV-A) isotherms of the PIMs.

A simple electrostatic model, based on the Helmholtz equation, that compares a closely packed monolayer of an amphiphilic compound (composed by a polar hydrophilic head and a long hydrocarbon tail) with a flat capacitor, could be used to gain insight into the properties of the LB films. In this model, the surface potential is given by $\Delta V = \frac{\mu_{\perp}}{\varepsilon_0 \varepsilon_r A} + \Psi_0$, where $\mu_{\perp}$ is the normal component of the dipole moment, ε_0 is the vacuum permittivity, ε_r is the relative dielectric constant, A is the area per molecule and Ψ_0 is the double-layer contribution that is only relevant for ionized films. The normal component of the dipole moment is the result of three contributions: the rearrangement of the interfacial water dipoles by the monolayer and the contribution of the dipoles of the hydrophilic heads and those of the hydrocarbon tails [14].

Of course, the structure of polymeric films is more complex than that of simple amphiphiles; however, some interesting conclusions can be deduced from experimental data. Positive and high ΔV values for PIM-EA-TB(H_2) suggest that the dipole moments in the film should mainly point to the normal to the water surface. Moreover, partial protonation of the amine groups of the Tröger's base at the air-water interface can be expected due to the acidification of the water subphase by the presence of CO_2 in the

atmosphere as it has been reported for other amines [15, 16]. For PIM-1 and PIM-TMN-Trip films there is no contribution from the double-layer to the surface potential and the low ΔV values observed for PIM-1 would be a consequence of the contorted 3D structure of the polymeric chains that have their dipole moments randomly oriented. Finally, the slightly negative ΔV values obtained for PIM-TMN-Trip would indicate that $\mu_{\perp}$ is low for the films of this polymer. Considering the 2D nature of this polymer (Fig. 1) and its plane of symmetry it can be deduced that dipole moments should be almost parallel to the water surface.

Brewster Angle Microscopy (BAM) images registered under compression (Figure 4) can provide valuable information about the formation of the polymeric films at the air-water interface.

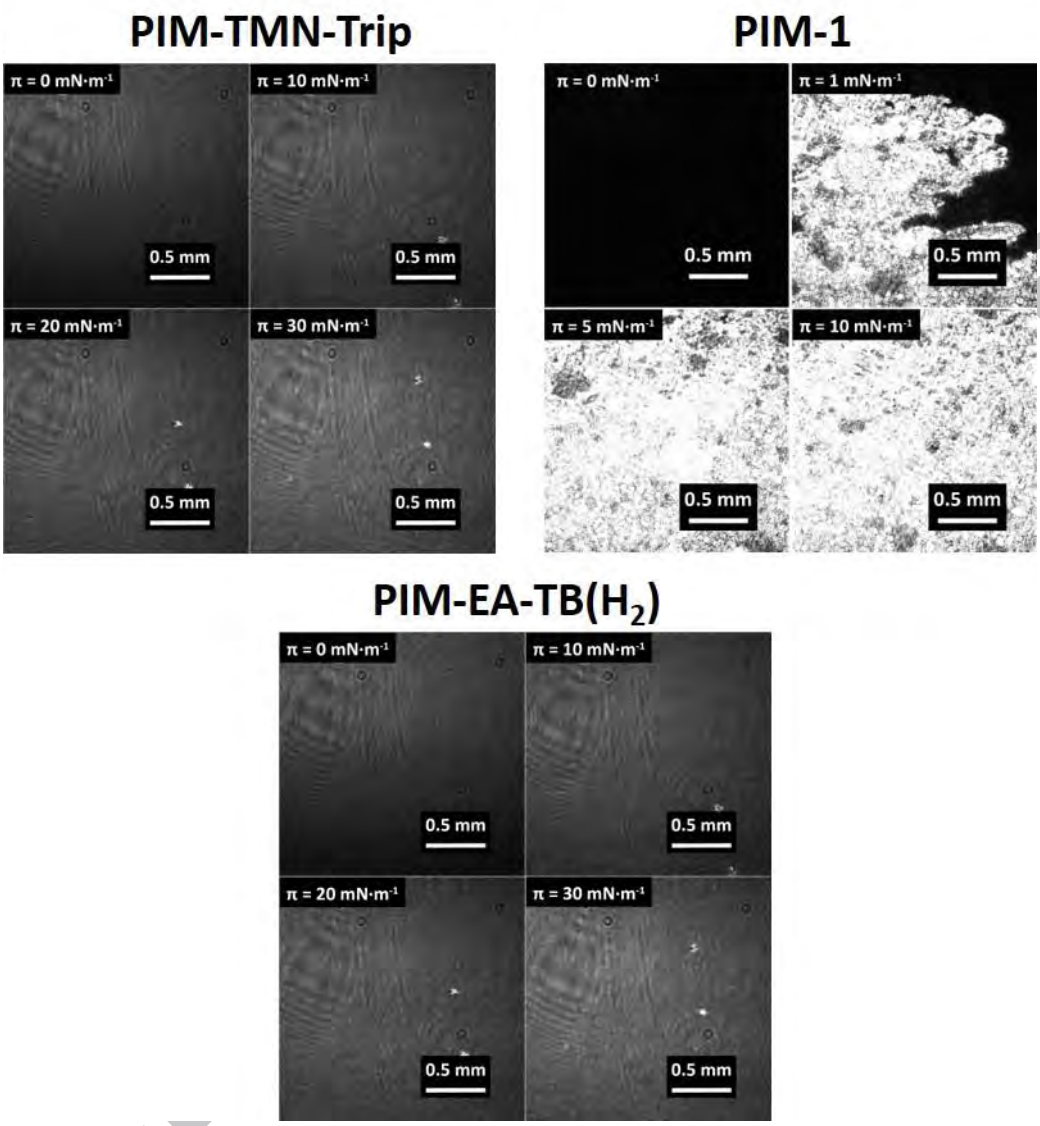

Figure 4. BAM images obtained during PIM films compression at the air-water interface.

Homogeneous and compact Langmuir films covering practically all the water surface at a surface pressure of ca. 10 $mN \cdot m^{-1}$ were obtained for PIM-TMN-Trip. For comparison, the BAM images for the previously reported PIM-EA-TB(H_2) were obtained and demonstrated similar features. Further compression of these films increased their thickness (images are brighter) which is consistent with a more compact packing of the polymers. In addition, both films were still homogenous at high surface pressures (30

$mN \cdot m^{-1}$). On the contrary, the PIM-1 images (Figure 4) show a brighter and less homogeneous film (i.e. domains with different thickness can be observed even at low surface pressures) than for the other two PIMs. BAM images are consistent with the π-A and ΔV-A isotherms discussed above and confirmed the relevance of the chemical structure of the PIMs in their behavior at the air-water interface. Moreover, the optimum range of surface pressures for the PIM transfer in order to obtain dense films, minimizing the formation of 3D aggregates, could be deduced from these studies. For PIM-TMN-Trip and PIM-EA-TB(H_2), the transference surface pressure range should be between 20-30 $mN \cdot m^{-1}$, whilst for PIM-1 it should be between 7-10 $mN \cdot m^{-1}$.

3.2. Supported PIM monolayer films

In a previous study [6], it was demonstrated that PIM-EA-TB(H_2) films transferred on a substrate by using the Langmuir-Schafer (LS) method at 30 $mN \cdot m^{-1}$ had a thickness of ca. 1 nm and several films could be successively deposited to obtain a PIM film with the desired thickness. In this study, LS films of PIM-TMN-Trip and PIM-1 have been transferred at 20 and 10 $mN \cdot m^{-1}$, respectively, on quartz and mica substrates and characterized using UV-vis spectroscopy and AFM. In addition, in order to analyze the effect of the transference method, the Langmuir-Blodgett (LB) technique has been used to transfer films of the three PIMs onto solid substrates at the same surface pressures as used for the LS films.

Figure 5 shows the UV-vis spectra for ultrathin LS and LB films (one layer) for the two new PIMs studied at 20 $mN \cdot m^{-1}$ (PIM-TMN-Trip) and 10 $mN \cdot m^{-1}$ (PIM-1) compared to the spectra of diluted chloroform solutions of the same polymers. These PIMs show bands in the 270-330 nm region and there are almost no changes in the position of these bands between solution, LS and LB films. Additionally, a broad band in the visible

region, at ca. 440 nm, attributed to the 1,4-dicyanobenzene unit [17]. This band is blue-shifted both in LB and in LS films respect to the solution spectrum. This hypsochromic shift (10 nm for PIM-1 and 20 nm for PIM-TMN-Trip) could indicate that the arrangement of the chromophores obtained for these polymers in ultrathin films corresponds to a lower energy conformation [18], this effect being more marked for PIM-TMN-Trip. Additionally, for these polymers, there are slight differences (2-4 nm) between the position of the wavelength of maximum absorbance in LB and LS films and the absorbance is slightly higher in LS than LB films. This reveal some changes in the polymer arrangement between the films fabricated by the LB and LS methods, as will be discussed below.

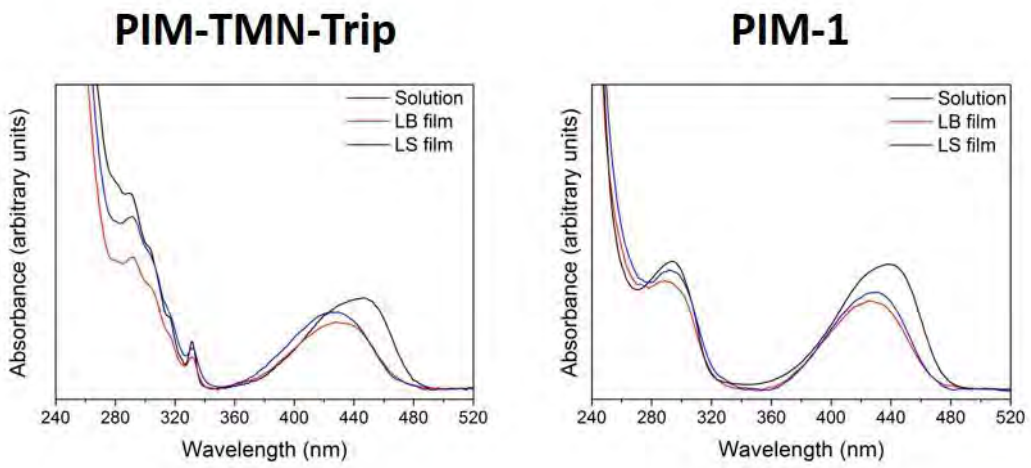

Figure 5. UV-vis spectra for LB and LS films (one layer) of the PIMs transferred at 20 $mN \cdot m^{-1}$ (PIM-TMN-Trip), 10 $mN \cdot m^{-1}$ (PIM-1) as well as for the corresponding diluted polymer solutions in chloroform.

The morphology, roughness and thickness of the PIM ultrathin films (one layer) transferred on mica were analyzed by AFM (Figure 6). The thicknesses of the films were determined measuring the height profile in different film borders and/or defects

(Figures S2 to S4 of the Supplementary Material). Table 1 summarizes the film root mean square roughness (RMS) and thickness values.

Substantial differences in terms of surface coverage [19] and film morphology [20] for polymeric films fabricated by the LB or LS transfer methods have been reported for other polymers such as polyanilines [20]. Generally, the LS method provides high quality deposition and faster monolayer transfer on large substrates, because the time required for substrate emersion/immersion at usual speed used in the LB method is very large.

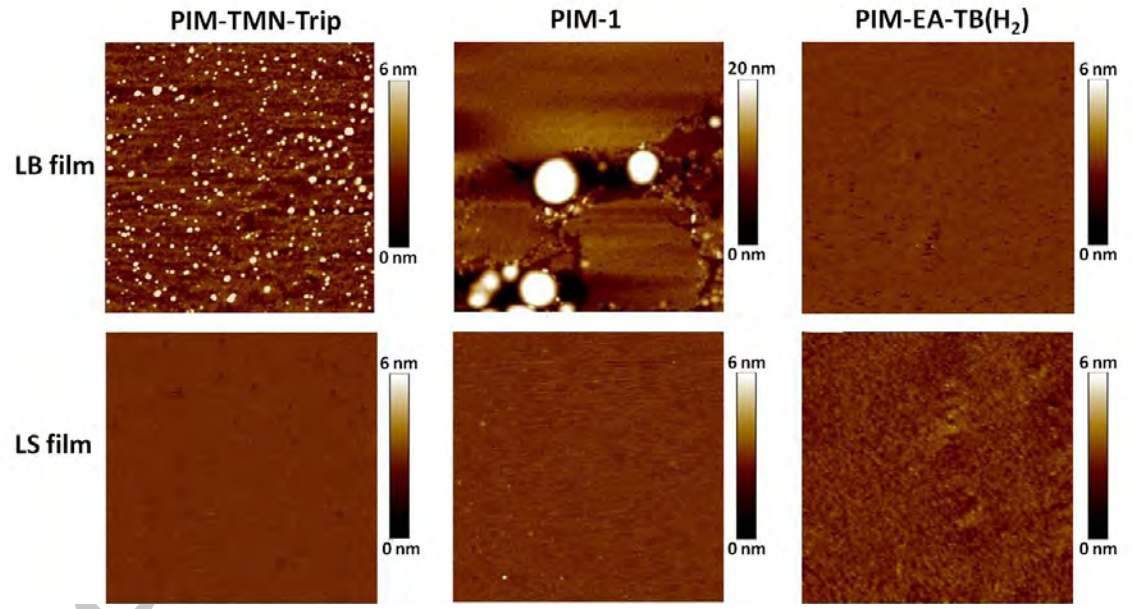

Figure 6. AFM images (size 2 × 2 μm) of ultrathin (one layer) LB and LS films of the three PIMs. Surface pressures of transference were: 20 $mN \cdot m^{-1}$ (PIM-TMN-Trip), 10 $mN \cdot m^{-1}$ (PIM-1) and 30 $mN \cdot m^{-1}$ (PIM-EA-TB(H_2)).

As can be observed in Figure 6, the morphologies of PIM-EA-TB(H_2) LB and LS films transferred at 30 $mN \cdot m^{-1}$ are very similar. Both LB and LS methods allow obtaining homogeneous and almost defect-free films and the corresponding root mean square

roughness (RMS) values are very low (Table 1). However, the LB film thickness is 2.2 times the LS film thickness (Table 1). Additionally, the UV-vis absorbance of the LS film at 297 nm is ca. 2.5 times higher than that of the LB film (Figure S5 of the Supplementary Material). These observations clearly reveal a different polymer arrangement in both films. In the LS film, the transition dipole moment of the polymer would be mainly parallel to the plane of the substrate, maximizing the interaction of the polymer with the incident radiation and leading to thickness film of 1 nm. On the contrary, in the LB film, the transition dipole moment would be tilted with respect to the substrate surface giving place to a higher film thickness and a decrease of the UV-vis absorbance.

Table 1. Root mean square roughness (RMS) and thickness for PIM ultrathin films (one layer) transferred at: 20 $mN \cdot m^{-1}$ (PIM-TMN-Trip), 10 $mN \cdot m^{-1}$ (PIM-1) and 30 $mN \cdot m^{-1}$ (PIM-EA-TB(H_2)).

	PIM-TMN-Trip		PIM-1		PIM-EA-TB(H_2)	
	LB film	LS film	LB film	LS film	LB film	LS film
RMS/nm	1.08	0.11	3.73	0.18	0.11	0.25
Thickness/nm	1.8	2.1	4.0	1.6	2.2	1.0

In the case of PIM-1, AFM images show significant differences between the morphology of LB and LS films. The LB film is formed by a homogenous layer of thickness ca. 4 nm which does not cover completely the substrate surface. In addition, thick accumulations of material (ca. 20 nm) with circular shape can be also seen at domain edges. On the contrary, very homogenous and defect-free films were obtained when the LS method was used. Moreover, LS films have a thickness of only 1.6 nm. The ratio between the thicknesses of the LB and LS films for PIM-1 (2.5) is a little

higher than the relationship obtained for PIM-EA-TB(H_2) films. This suggests that the orientation of the polymeric chains for these PIMs depends significantly on the transfer method. However, for PIM-1 the absorbance for a LS film at 430 nm is ca. 1.2 times the LB film absorbance which is not in agreement to the thickness ratio, probably due to the presence of the above mentioned thick accumulations of material in LB films which contribute significantly to increase their absorbance.

Finally, the AFM images for LB and LS films of PIM-TMN-Trip show homogenous films with similar thicknesses, 1.8 and 2.1 nm, respectively, although the RMS is higher for the LB film (Table 1) due to the presence of small accumulations of material homogeneously distributed. It should be highlighted that the height (ca. 4 nm) and size of these polymer accumulations are significantly lower than for PIM-1 (ca. 20 nm). Additionally, both films present similar absorbance in the UV-vis spectrum (Figure 5) indicating that, although the transfer method could produce differences in the arrangement of the PIMs in the films, these differences are scarce for the 2D macromolecular chains of PIM-TMN-Trip.

3.3. PIM multilayer films deposited onto solid substrates: gas separation studies

The characterization of PIM monolayer films deposited on solid substrates has shown that the LS method allows obtaining more compact, homogeneous and thicker PIM films than the LB method. In order to fabricate ultrathin PIM supported membranes of the desired thickness, a controlled number of PIM films should be deposited on PTMSP supports. In this sense, it is crucial to characterize the successive depositions of the PIM on a solid substrate.

PIM-1 and PIM-TMN-Trip multilayer films were transferred onto quartz substrates at 10 and 20 $mN \cdot m^{-1}$, respectively, and the corresponding UV-vis spectra were acquired

after each deposition. As can be observed in Figure 7, the successive depositions of PIM-TMN-Trip showed a constant increase in the absorbance of the film with the number of layers, indicating a continuous and constant polymer deposition for PIM-TMN-Trip. A similar result was obtained in a previous study for PIM-EA-TB(H_2). However, for PIM-1, the increment of the film absorbance with the successive depositions was constant only up to 10 layers. Further transferences increase the absorbance of the film, but the slope was reduced, which suggests either that the amount of polymer transferred is reduced or that a change in the orientation of the polymer chains takes place when more than 10 layers are deposited. This can be probably due to the contorted nature of the 3D PIM-1 chains that are forming domains with different thickness at the air-water interface that does not facilitate the compact packing of several PIM layers. However, PIM-TMN-Trip and PIM-EA-TB(H_2) form homogeneous and compact Langmuir films and can be successively deposited on solid substrate.

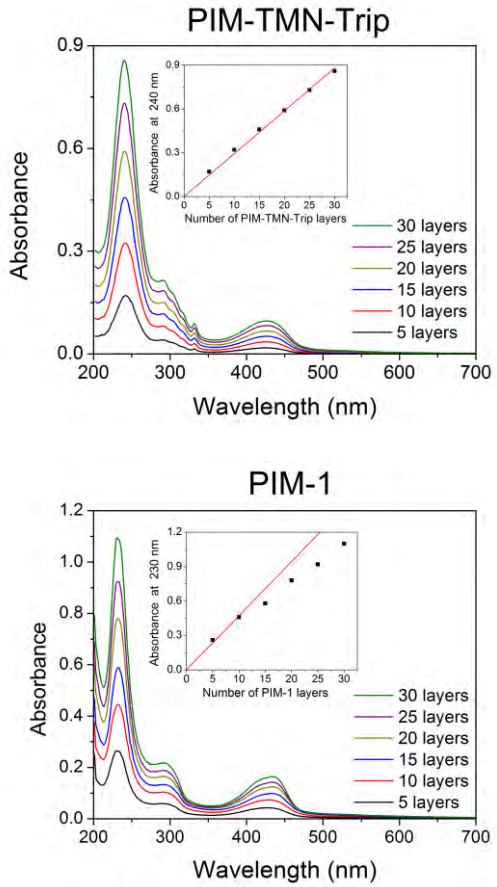

Figure 7. UV-vis spectra for several LS depositions of PIM-TMN-Trip and PIM-1 on quartz at 20 $mN \cdot m^{-1}$ and 10 $mN \cdot m^{-1}$, respectively. (Insets: absorbance at the indicated wavelength vs. number of polymer layers deposited).

The separation performance of a series of PTMSP/PIM-TMN-Trip and PTMSP/PIM-1 composite membranes incorporating 15, 20 and 30 PIM monolayers was tested for their potential in CO_2/N_2 separation for post-combustion carbon capture (temperature 35 ºC; feed pressure 1-3 bar; CO_2/N_2 mixture composition in volume 10/90). PTMSP is a regular component of the gutter layer in composite membranes [2] and it has been previously used for LB film deposition [21] because its solvent cast membranes present an almost flat surface and very high gas permeability [22]. Gas permeability and selectivity for each of the membranes are shown in Figure 8. Dense PTMSP membranes (thickness ca. 80 µm) show high CO_2 permeance (435 GPU at 1 bar) but low CO_2/N_2 selectivity (4.2), while composite PTMSP/PIM-TMN-Trip membranes show a gradual

increase of CO_2/N_2 selectivity with the number of PIM monolayers deposited and a regular decrease in CO_2 permeance, following a similar trend than PTMSP/PIM-EA-TB(H_2) composite membranes previously studied [6]. Moreover, when the feed pressure increased from 1 to 3 bar, the CO_2/N_2 selectivity values diminished by ca. 7% in composite membranes containing 15 PIM-TMN-Trip monolayers but this reduction was between 3-4% when 20 or 30 PIM-TMN-Trip films were deposited (Table S1 of the Supplementary Material and Figure 8). This suggests that it is necessary to deposit at least 20 monolayers to obtain an almost defect-free ultrathin PIM-TMN-Trip selective layer on top of the PTMSP support, as it was also reported for PTMSP/PIM-EA-TB(H_2) composite membranes [6].

PTSMP/PIM-TMN-Trip membranes incorporating 30 PIM monolayers present a CO_2/N_2 selectivity of 12.1 at 1 bar, that is close to the ideal CO_2/N_2 selectivity value (14.9) recently reported for a methanol-treated dense membrane of pure PIM-TMN-Trip [13]. In a previous study it was shown for PTMSP/PIM-EA-TB(H_2) composite membranes that the ideal selectivity was 35% higher than the selectivity obtained with CO_2/N_2 mixtures in volume proportion 10/90 [6]. Although the CO_2 permeance for this PTSMP/PIM-TMN-Trip composite membranes (134 GPU) is lower than the CO_2 single gas permeance reported for the pure PIM-TMN-Trip membrane [13] (171 GPU, applying the thickness of 195 μm to the reported CO_2 permeability of 33300 Barrer), it is higher than the CO_2 permeance of composite PTMSP/PIM-EA-TB(H_2) membranes (114 GPU) of similar selectivity [6].

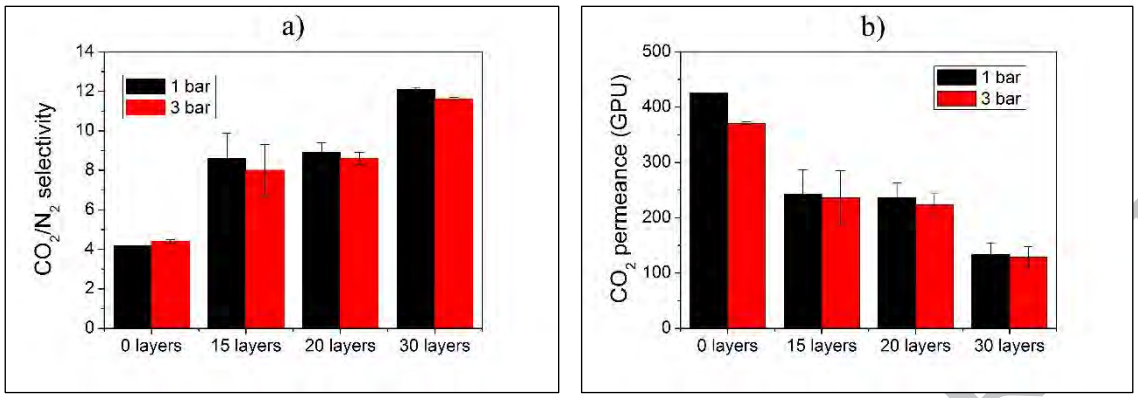

Figure 8. CO_2/N_2 selectivity (a) and CO_2 permeance (b) of polymeric membranes: bare PTMSP (0 layers) and composite membranes formed by 15-30 LS PIM-TMN-Trip films deposited onto PTMSP. Error bars were obtained from measurements of at least 2 membrane samples of each type.

When PTMSP/PIM-1 composite membranes containing up to 30 PIM-1 monolayers were tested in the same conditions, a significant decrease in CO_2 permeance compared to pure PTMSP was obtained, but CO_2/N_2 selectivity values do not improve significantly over the performance of pure PTMSP, revealing that it was not possible to obtain an effective selective layer with PIM-1 using this methodology. This can be related with the difficulty to keep a constant polymer deposition for a large number of PIM-1 layers, as discussed in UV-vis characterization.

In order to obtain more information about the separation properties of the PIM ultrathin films, a model of resistances in series [23] was applied to analyze composite PTSMP/PIM-TMN-Trip membranes. In this model, the overall measured permeance of the membrane (in GPU) is given by: $\frac{1}{P_{overall}} = \frac{1}{P_{PTMSP}} + \frac{1}{P_{PIM}}$, where $P_{overall}$, P_{PTMSP} and P_{PIM} are, respectively, the permeances of the composite membrane, the PTMSP support and the PIM ultrathin layer, respectively. $P_{overall}$ and P_{PTMSP} were obtained from permeance values reported on Table S1 (assuming that composite membranes and pure

PTMSP membranes have the same thickness) and, therefore, P_{PIM} were calculated for all the membranes and pressures (see Table S2 of the Supplementary Material). Since the thickness of one single PIM layer is known (2.1 nm), the CO_2 and N_2 permeabilities (in barrer) were calculated multiplying the permeance in GPU by the corresponding thickness of the PIM ultrathin layer and the CO_2/N_2 selectivities were obtained from the ratio of permeabilities. From these calculations, it can be estimated (at 1 bar) an average CO_2 permeability of 17.5 barrer for the PIM ultrathin layer with a CO_2/N_2 selectivity of 16.6. This means that the gas permeability is somewhat less than the values obtained for thicker membranes of the same polymer, probably due to the compact PIM packing in the LS films, but the separation capacity is conserved.

Additionally, aged composite membranes were tested for gas separation 18 months after their first use. Three PTSMP/PIM-TMN-Trip membranes incorporating, respectively, 15, 25 and 30 PIM monolayers were studied and the results are shown in Table S3 of the Supplementary Material. It can be noticed that the CO_2 permeance of aged membranes have decreased to ca. one third of their initial value while the CO_2/N_2 selectivity followed the opposite tendency, reaching values 1.5-fold higher. Both results are indicative of polymer aging. This is consistent with previous long-term assessment of physical aging of the gas transport in PIM-1. In fact, Bernardo et al. [24] observed a reduction of the gas permeability of six different gases (including CO_2 and N_2) as a function of time, while confirming the gas separation selectivity increase of the aged membranes (> 5 years).

Finally, it should be mentioned that the LS transfer based methodology used to prepare PTMSP/PIM composite membranes allows an important reduction of the PIM content in the membrane [6]. A simple comparison between the thickness of the PIM-TMN-Trip used for the fabrication of the ultrathin selective layer in PTSMP/PIM-TMN-Trip

composite membranes (thickness of the selective layer = 30 monolayers × 2.1 nm = 63 nm) and that of the dense PIM-TMN-Trip membrane (of the same thickness than the composite membrane, ca. 80 μm) shows that the PIM content in the composite membranes is only 0.08 % of that of the PIM dense membrane. Moreover, we have shown that PIM chemical structure and transfer method determine the arrangement of polymeric chains in ultrathin films, since a compact and homogenous deposition in the successive film transfer is necessary to obtain ultrathin PIM selective layers.

4. Conclusions

The formation of polymer films at the air-water interface has been investigated for two polymers of intrinsic microporosity with very different chain conformations: PIM-1 that presents a contorted 3D structure and PIM-TMN-Trip formed by 2D chains. The information obtained from π-A and ΔV-A isotherms and BAM images collected during film compression has revealed that the behavior of these polymers at the air-water interface strongly depends on the structure of the polymer chains. Thin and homogeneous monolayers are obtained with PIM-TMN-Trip while PIM-1 forms thicker and less uniform films.

Polymer films have been transferred on different solid substrates using the vertical (LB) and horizontal (LS) deposition methods and the films obtained have been characterized by AFM and UV-vis spectroscopy. The AFM study showed that there are significant differences in the structure of PIM-1 LB and LS films, with LB films at least two times thicker than LS films. However, LB and LS films of the 2D polymer PIM-TMN-Trip are similar. Additionally, LB films fabricated with PIM-1 are significantly rougher than LS films due to the presence of thicker domains in the LB films that were not observed in the LS films. These features, together with the differences in film absorbance

determined by UV-vis spectroscopy, reveal that the orientation of the 3D PIM-1 chains depends significantly on the transfer method while the 2D PIM-TMN-Trip presents similar organization in LB and LS films. Moreover, we concluded that the LS methodology is more efficient for the fabrication of PIM multilayer films onto solid substrates than the LB method, as it has been reported before for other polymers [20].

Finally, PTMSP/PIM-TMN-Trip composite membranes were obtained by depositing a controlled number of PIM monolayers onto flat PTMSP supports using the LS methodology and these membranes were tested for CO_2/N_2 separation. The composite membranes containing 30 monolayers of PIM-TMN-Trip have demonstrated high CO_2 permeance and moderate CO_2/N_2 separation with its permselectivity performance similar to that of the corresponding dense membrane but was prepared by using only a small fraction of the selective polymer (less than 0.1%).

This study highlights the relevance of polymer design in order to obtain homogenous films with a 2D chain structure clearly beneficial. It is likely that the previously reported success [6] of the film-forming ability of the 3D contorted PIM-EA-TB(H_2) is due to the presence of amine groups [16] within the TB unit resulting in strong adhesion of the polymer layer to the water surface. In future works, new PIMs with a 2D structure and containing other functional groups will be synthesized and assembled into thin films in order to improve their gas separation performance.

Acknowledgements

The research leading to these results has received funding from the EU PF7 Programme (FP7/2007-2013), under grant agreement number 608490, project M4CO2. Financial support from the Spanish MINECO and FEDER (MAT2016-77290-R), the Aragón Government (E31_17R and T43_17R) and the ESF is gratefully acknowledged. J. S.-L. thanks the Spanish Education Ministry Program FPU2014 for his PhD grant. All the

microscopy work was done in the Laboratorio de Microscopías Avanzadas at the Instituto de Nanociencia de Aragón (LMA-INA). Finally, the authors would like to acknowledge the use of the Servicio General de Apoyo a la Investigación-SAI, Universidad de Zaragoza.

References

[1] M. Galizia, W.S. Chi, Z.P. Smith, T.C. Merkel, R.W. Baker, B.D. Freeman, 50th Anniversary Perspective: Polymers and Mixed Matrix Membranes for Gas and Vapor Separation: A Review and Prospective Opportunities, Macromolecules 50(20) (2017) 7809-7843.

[2] Z. Dai, L. Ansaloni, L. Deng, Recent advances in multi-layer composite polymeric membranes for CO_2 separation: A review, Green Energy & Environment 1(2) (2016) 102-128.

[3] R.W. Baker, B.T. Low, Gas Separation Membrane Materials: A Perspective, Macromolecules 47(20) (2014) 6999-7013.

[4] N.B. McKeown, P.M. Budd, Polymers of intrinsic microporosity (PIMs): organic materials for membrane separations, heterogeneous catalysis and hydrogen storage, Chemical Society Reviews 35(8) (2006) 675-683.

[5] N.B. McKeown, P.M. Budd, Exploitation of Intrinsic Microporosity in Polymer-Based Materials, Macromolecules 43(12) (2010) 5163-5176.

[6] J. Benito, J. Sanchez-Lainez, B. Zornoza, S. Martin, M. Carta, R. Malpass-Evans, C. Tellez, N.B. McKeown, J. Coronas, I. Gascon, Ultrathin Composite Polymeric Membranes for CO_2/N_2 Separation with Minimum Thickness and High CO_2 Permeance, ChemSusChem 10(20) (2017) 4014-4017.

[7] K. Ariga, Y. Yamauchi, T. Mori, J.P. Hill, 25th Anniversary Article: What Can Be Done with the Langmuir-Blodgett Method? Recent Developments and its Critical Role in Materials Science, Advanced Materials 25(45) (2013) 6477-6512.

[8] J.Y. Park, R.C. Advincula, Nanostructuring polymers, colloids, and nanomaterials at the air-water interface through Langmuir and Langmuir-Blodgett techniques, Soft Matter 7(21) (2011) 9829-9843.

[9] P.M. Budd, B.S. Ghanem, S. Makhseed, N.B. McKeown, K.J. Msayib, C.E. Tattershall, Polymers of intrinsic microporosity (PIMs): robust, solution-processable, organic nanoporous materials, Chemical Communications (2) (2004) 230-231.

[10] P.M. Budd, E.S. Elabas, B.S. Ghanem, S. Makhseed, N.B. McKeown, K.J. Msayib, C.E. Tattershall, D. Wang, Solution-processed, organophilic membrane derived from a polymer of intrinsic microporosity, Advanced Materials 16(5) (2004) 456-459.

[11] M. Carta, R. Malpass-Evans, M. Croad, Y. Rogan, J.C. Jansen, P. Bernardo, F. Bazzarelli, N.B. McKeown, An Efficient Polymer Molecular Sieve for Membrane Gas Separations, Science 339(6117) (2013) 303-307.

[12] E. Tocci, L. De Lorenzo, P. Bernardo, G. Clarizia, F. Bazzarelli, N.B. McKeown, M. Carta, R. Malpass-Evans, K. Friess, K. Pilnacek, M. Lanc, Y.P. Yampolskii, L. Strarannikova, V. Shantarovich, M. Mauri, J.C. Jansen, Molecular Modeling and Gas Permeation Properties of a Polymer of Intrinsic Microporosity Composed of Ethanoanthracene and Troger's Base Units, Macromolecules 47(22) (2014) 7900-7916.

[13] I. Rose, C.G. Bezzu, M. Carta, B. Comesana-Gandara, E. Lasseuguette, M.C. Ferrari, P. Bernardo, G. Clarizia, A. Fuoco, J.C. Jansen, K.E. Hart, T.P. Liyana-Arachchi, C.M. Colina, N.B. McKeown, Polymer ultrapermeability from the inefficient packing of 2D chains, Nature Materials 16(9) (2017) 932-938.

[14] O.N. Oliveira, C. Bonardi, The surface potential of Langmuir monolayers revisited, Langmuir 13(22) (1997) 5920-5924.

[15] O. Albrecht, H. Matsuda, K. Eguchi, Main and tilt transition in octadecylamine monolayers, Colloids and Surfaces A-Physicochemical and Engineering Aspects 284 (2006) 166-174.

[16] W. Sung, Z. Avazbaeva, D. Kim, Salt Promotes Protonation of Amine Groups at Air/Water Interface, Journal of Physical Chemistry Letters 8(15) (2017) 3601-3606.

[17] B. Satilmis, P.M. Budd, Base-catalysed hydrolysis of PIM-1: amide versus carboxylate formation, RSC Advances 4(94) (2014) 52189-52198.

[18] G. Pera, A. Villares, M.C. Lopez, P. Cea, D.P. Lydon, P.J. Low, Preparation and characterization of Langmuir and Langmuir-Blodgett films from a nitrile-terminated tolan, Chemistry of Materials 19(4) (2007) 857-864.

[19] C.P.L. Rubinger, R.L. Moreira, B.R.A. Neves, L.A. Cury, C.A. Ferreira, A. Meneguzzi, AFM studies of poly (5-amino-1-naphthol) ultrathin tilms obtained by associating Langmuir-Schaefer and Langmuir-Blodgett methods, Synthetic Metals 145(2-3) (2004) 147-151.

[20] V.I. Troitsky, T.S. Berzina, M.P. Fontana, Deposition of uniform conductive polyaniline films and approach for their patterning, Synthetic Metals 129(1) (2002) 39-46.

[21] M.H. Wang, V. Janout, S.L. Regen, Gas Transport across Hyperthin Membranes, Accounts of Chemical Research 46(12) (2013) 2743-2754.

[22] T. Masuda, E. Isobe, T. Higashimura, K. Takada, Poly[1-(Trimethylsilyl)-1-Propyne] a New High Polymer Synthesized with Transition-Metal Catalysts and Characterized by Extremely High Gas-Permeability, Journal of the American Chemical Society 105(25) (1983) 7473-7474.

[23] D.L. Meixner, P.N. Dyer, Characterization of the transport properties of microporous inorganic membranes, Journal of Membrane Science 140(1) (1998) 81-95.

[24] P. Bernardo, E. Bazzarelli, F. Tasselli, G. Clarizia, C.R. Mason, L. Maynard-Atem, P.M. Budd, M. Lanc, K. Pilnacek, O. Vopicka, K. Friess, D. Fritsch, Y.P. Yampolskii, V. Shantarovich, J.C. Jansen, Effect of physical aging on the gas transport and sorption in PIM-1 membranes, Polymer 113 (2017) 283-294.

GRAPHICAL ABSTRACT